第32卷 第8期 焊 接 学 报 Vol. 32 No. 8
2011年8月 TRANSACTIONS OF THE CHINA WELDING INSTITUTION August 2011

7A52铝合金搅拌摩擦焊焊缝第二相分析及微区电位测试

张 平，李 奇，赵军军
（装甲兵工程学院 装备再制造技术国防科技重点实验室，北京 100072）

张 平

摘 要： 7A52铝合金搅拌摩擦焊焊缝第二相的种类、大小、分布和电位等都对材料的腐蚀行为有重要的影响. 采用光学显微镜、扫描电镜、能谱分析仪、扫描开尔文探针力显微镜分析了焊缝中的第二相，并测试了其微区电位. 结果表明，焊缝各区域第二相的组成主要为弥散分布的AlFeMnSi和Mg_2Si，它们的尺寸约为几微米，电位都低于基体. Mg_2Si的电位值低于AlFeMnSi，故在腐蚀环境中，Mg_2Si更容易腐蚀. 这为深入分析7A52铝合金搅拌摩擦焊焊缝的腐蚀行为奠定了基础.

关键词： 7A52铝合金；搅拌摩擦焊；焊缝；第二相；微区电位
中图分类号： TG453 **文献标识码：** A **文章编号：** 0253－360X(2011)08－0042－03

0 序 言

7A52铝合金(曾用名LC52，5210)是一种高强铝合金，具有较高的比强度、较好的断裂韧度和抗低周疲劳性能[1]，是列入国家军用标准的唯一铝合金，已在军用装备与军用设施、建筑等领域获得批量应用. 利用搅拌摩擦焊技术(friction stir welding，FSW)对7A52铝合金进行焊接，其焊缝的性能较熔焊有大幅度提高[2-4].

焊缝中的第二相与基体的化学成分、电化学性质不同，在腐蚀环境中会形成腐蚀微电偶加速局部腐蚀. 在分析焊缝第二相组成的基础上，利用扫描开尔文探针力显微镜(scanning Kelvin probe force microscopy，SKPFM)对第二相进行了微区电位测试，确定了第二相的电位，探讨了其在局部腐蚀过程中的影响程度. 研究结果对理解焊缝局部腐蚀起始点处的电化学行为有着重要的意义.

1 试验方法

试验所用材料为西南铝业集团公司生产8 mm厚7A52铝合金板材，材料为淬火人工时效状态，其化学成分见表1. 搅拌摩擦焊试验在立式铣床改造的焊接设备上进行. 试验采用自制的螺旋形搅拌头，其轴肩直径为20 mm，搅拌针根部直径为7 mm. 搅拌头旋转频率为25 r/s，焊接速度为60 mm/min，倾斜角为1°，下压量0.15 mm. 对焊缝横向取样，经Keller's试剂浸蚀，利用(OLYMPUS) BX2M光学显微镜对焊缝的显微组织进行观察. 用Quanta 250型扫描电子显微镜观察第二相的形貌和分布，用能谱仪分析其成分. 使用美国Veeco公司的Dimension™ V扫描开尔文探针力显微镜测试第二相的电位[5-8].

表1 7A52铝合金的化学成分(质量分数，%)
Table 1 Chemical compositions of 7A52 Al alloy

Zn	Mg	Mn	Cr	Ti	Zr	Cu	Fe	Si	Al
4.35	2.40	0.35	0.20	0.12	0.10	0.12	<0.30	<0.25	余量

2 试验结果与分析

2.1 焊缝第二相分析

7A52铝合金FSW焊缝横截面可以划分为三个区域：即动态再结晶区(dynamically recrystallized zone，DRZ)，热力影响区(thermal-mechanical affected zone，TMAZ)，热影响区(heat affected zone，HAZ).

图1为7A52铝合金FSW焊缝的显微组织. DRZ的显微组织如图1a所示. 该区域由于受到搅拌头强烈的旋转搅拌和搅拌摩擦热的共同作用，达到再结晶温度，发生动态再结晶，基材的板条状组织完全转变为等轴晶粒，晶粒尺寸非常细小，大小约为1～2 μm. 图1b，c为TMAZ的显微组织. 该区域的

收稿日期：2010－06－07
基金项目：国家自然科学基金资助项目(50801066)

组织在热循环和机械搅拌作用下,发生了晶粒粗化和弯曲变形,由基材的细板条状组织变为具有一定弧度的粗板条状组织. 图 1d 为 HAZ 的显微组织.

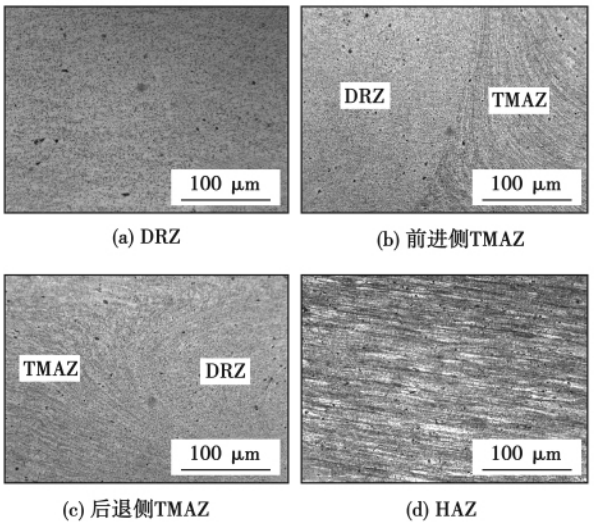

图 1　7A52 铝合金 FSW 焊缝的显微组织

Fig. 1　Microstructure of FSW seam of 7A52 Al alloy

从显微组织可以看出,该区域的组织与母材类似,但是晶粒发生了粗化.

图 2a 是 DRZ 的 SEM 背散射电子形貌. 由于搅拌摩擦热使该区域的温度升高,使第二相发生部分溶解,所以与母材相比,它们的长度变为几微米[9]. 图 2 中灰色的第二相 a 包含 Al,Fe,Mn,Si 元素,原子含量为 77.4% Al,11.66% Fe,5.19% Mn,5.75% Si. b,c 的能谱分析结果与 a 相似,均含有 Al,Fe,Mn,Si 元素,该类相为 AlFeMnSi. 黑色的第二相 d 包含 Al, Mg,Si 元素,原子含量为 30.89% Al,32.52% Mg,36.60% Si. 由于镁和硅在 7A52 铝合金中只能以 Mg_2Si 的形式化合,因此该类相为 Mg_2Si. TMAZ 和 HAZ 第二相的组成和形貌与 DRZ 类似,并无明显变化. 由以上分析可以看出,7A52 铝合金FSW焊缝的第二相可分为两类: AlFeMnSi 和 Mg_2Si.

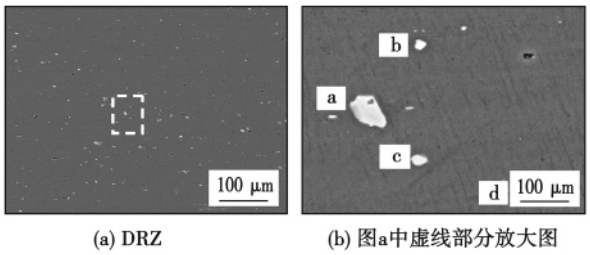

图 2　DRZ 的 SEM 背散射电子形貌

Fig. 2　Back scattered electron image of DRZ

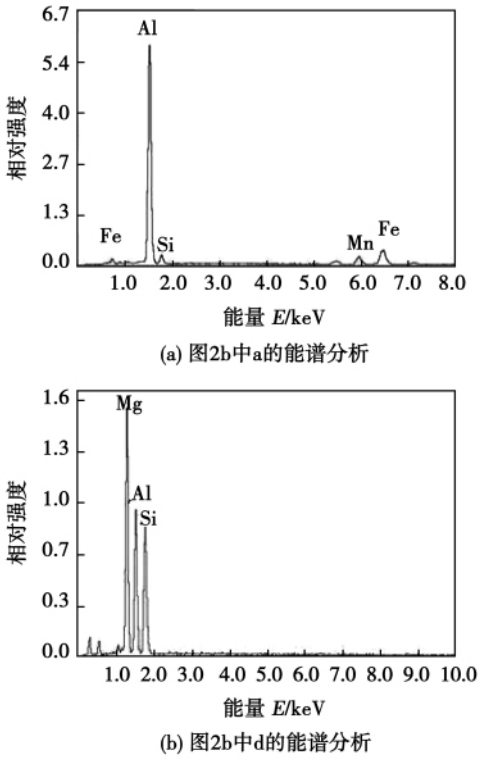

图 3　DRZ 第二相的能谱分析

Fig. 3　EDS analysis of second phases in DRZ

2.2　焊缝第二相的微区电位

图 4a 是利用 SKPFM 测试 DRZ 不同尺寸 Al –

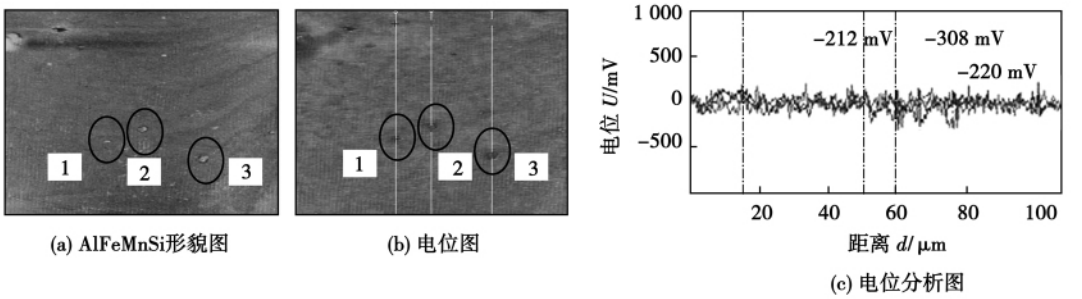

图 4　不同尺寸 AlFeMnSi 的微区电位测试图

Fig. 4　Volta potential maps of AlFeMnSi intermetallics with different sizes

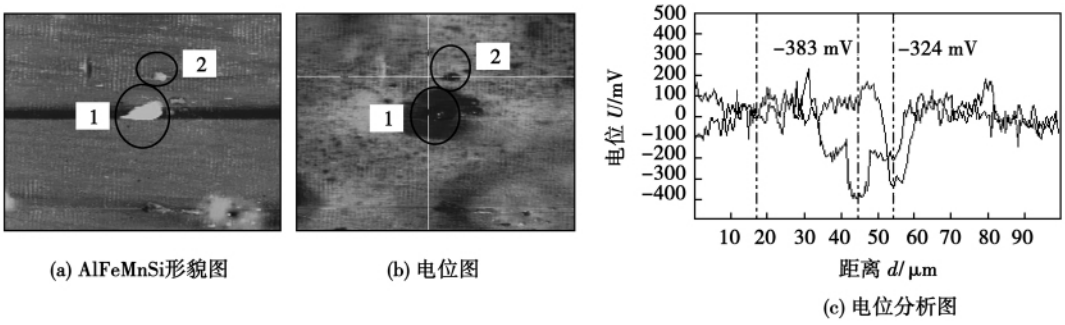

(a) AlFeMnSi形貌图 (b) 电位图 (c) 电位分析图

图 5 不同尺寸 Mg_2Si 的微区电位测试图

Fig. 5 Volta potential maps of Mg_2Si intermetallics with different sizes

FeMnSi 的形貌图，图 4 中 1 号 AlFeMnSi 的尺寸约为 2.9 μm，2 号的尺寸约为 3.1 μm，3 号的尺寸约为 4.3 μm. 图 4b 中 AlFeMnSi 相对基体呈暗色，表明其相对基体呈阳极. 图 4c 中最左侧的垂直虚线代表基体的电位，3 个 AlFeMnSi 相对基体的电位分别约为 -212，-308，-220 mV. 如图 5 所示，1 号 Mg_2Si 的尺寸约为 15 μm，相对基体的电位约为 -383 mV；2 号 Mg_2Si 的尺寸约为 5 μm，相对基体的电位约为 -324 mV. 由此可见，同类相的尺寸不同，相对基体的电位值也不同.

3 结 论

(1) 7A52 铝合金 FSW 焊缝第二相的组成主要为 AlFeMnSi 和 Mg_2Si.

(2) FSW 焊缝中 AlFeMnSi 和 Mg_2Si 的电位均低于基体，AlFeMnSi 相对基体的电位平均值约为 -247 mV，Mg_2Si 相对基体的电位平均值约为 -353 mV. 而且同类相的尺寸不同，相对基体的电位值也不同. Mg_2Si 相对基体的电位值很低，在腐蚀环境中容易造成点蚀，影响焊缝的耐腐蚀性能.

参考文献:

[1] 陈康华，黄兰萍，郑 强，等. 高温预析出对 7A52 合金应力腐蚀性能的影响 [J]. 中国有色金属学报，2005，15(3)：441-445.
Chen Kanghua，Huang Lanping，Zheng Qiang，*et al*. Effect of high-temperature pre-precipitation on stress corrosion cracking of 7A52 alloy [J]. The Chinese Journal of Nonferrous Metals，2005，15(3)：441-445.

[2] 傅志红，贺地求，周鹏展，等. 7A52 铝合金搅拌摩擦焊焊缝的组织分析 [J]. 焊接学报，2006，27(5)：65-68.
Fu Zhihong，He Diqiu，Zhou Pengzhan，*et al*. Structure investigation of friction stir welding of 7A52 aluminum alloy [J]. Transactions of the China Welding Institution，2006，27(5)：65-68.

[3] 周鹏展，钟 掘，贺地求. 7A52 铝合金厚板搅拌摩擦焊 [J]. 中国有色金属学报，2006，16(6)：964-969.
Zhou Pengzhan，Zhong Jue，He Diqiu. Friction-stir welding on thick plate of 7A52 aluminum alloy [J]. The Chinese Journal of Nonferrous Metals，2006，16(6)：964-969.

[4] 刘红伟，周 琦，朱 军，等. 7A52 铝合金厚板搅拌摩擦焊接头性能研究 [J]. 兵器材料科学与工程，2006，29(3)：57-60.
Liu Hongwei，Zhou Qi，Zhu Jun，*et al*. Research on joint properties of 7A52 aluminum alloy thick plate by friction stir welding [J]. Ordnance Material Science and Engineering，2006，29(3)：57-60.

[5] Andreatta F，Apachitei I，Kodentsov A A，*et al*. Volta potential of second particles in extruded AZ80 magnesium alloy [J]. Electrochimica Acta，2006，51：3551-3557.

[6] Lacroix L，Ressier L，Blanc C，*et al*. Statistical study of the corrosion behavior of Al2CuMg intermetallics in AA2024-T351 by SKPFM [J]. Journal of the Electrochemical Society，2008，155(1)：C8-C15.

[7] De Wit J H W. Local potential measurements with the SKPFM on aluminium alloys [J]. Electrochimica Acta 2004，49：2841-2850.

[8] Musterz T H，Hughes A E. Applications and limitations of scanning Kelvin probe force microscopy for the surface analysis of aluminum alloys [J]. Journal of the Electrochemical Society，2006，153(11)：B474-B485.

[9] Paglia C S，Jata K V，Buchheit R G. A cast 7050 friction stir weld with scandium：microstructure，corrosion and environmental assisted cracking [J]. Materials Science and Engineering A，2006，424：196-204.

作者简介： 张 平，男，1958 年出生，博士，教授，博士研究生导师. 主要从事焊接和真空镀膜等表面工程技术研究. 发表论文 100 余篇. Email：zhangp5801@sina.com

tions are researched. The results are discussed properly and verified. The calculated results are in agreement with the experimental-measured values.

Key words: T-joint; finite element simulation; thermal transfer coefficient; temperature distribution

Characteristics of metal deposited by laser-MAG hybrid welding with HS-80 welding wire LEI Zhen[1], TENG Bin[1], WANG Xuyou[1], ZHAO Xudong[2] (1. Harbin Welding Institute, China Academy of Machinery Science & Technology, Harbin 150080, China; 2. Liebherr Machinery (Dalian) Co., Ltd., Dalian 116600, China). p 37 - 41

Abstract: The mechanical properties and welding metallurgy laws of deposited metal of HS-80 welding wire by laser-MAG hybrid welding and MAG welding were studied. The results showed that the yield strength, tensile strength and impact work of the deposited metal by laser-MAG hybrid welding were all enhanced observably compared with those by MAG welding, and the microstructure was finer. Meanwhile the alloying element transition coefficient of laser-MAG hybrid welding was increased. In the laser-MAG hybrid welding process, the weld puddle cooled quickly at the high welding speed and the laser beam made the weld puddle flow acutely. These two technology factors were the main reasons of grain refinement. Moreover the content increasing of some elements such as Ti and Mo, which can make grain finer, was another reason of grain refinement. The grain refinement of the microstructure and the content of alloying elements increasing due to the improving of alloying element transition coefficient were the main reasons that enhanced the toughness and mechanical strength of deposited metal by laser-MAG hybrid welding.

Key words: welding wire for low alloy high strength steel; deposited metal; laser; hybrid welding

Analysis and volta potential measurement of second phases in friction stir welding seam of 7A52 aluminum alloy ZHANG Ping, LI Qi, ZHAO Junjun (National Defense Key Laboratory for Remanufacturing Technology, Academy of Armored Forces Engineering, Beijing 100072, China). p 42 - 44

Abstract: The species, size and volta potential of intermetallics of friction stir welding seam of 7A52 aluminum alloy have important influence on its corrosion behavior. The interemtallics of the welded seam were observed and characterized with metallographic microscope, scanning electron microscope, energy dispersive spectrometer and scanning Kelvin probe force microscope, and the volta potential of the welded seam was tested. The results indicate that the irregularly shaped intermetalics Al-FeMnSi and Mg_2Si disperse in the welded seam, which sizes are several microns and volta potentials are lower than the matrix. The volta potential of Mg_2Si is lower than that of AlFeMnSi intermetalics, which means that Mg_2Si is easier to be corroded in erosive environments. The results lay the foundation of studying corrosion behavior of friction stir welding seam of 7A52 aluminum alloy.

Key words: 7A52 aluminum alloy; friction stir welding; welded seam; intermetallics; volta potential

Tracer investigation of convection in weld pool under TIG welding process LI Dongjie, LU Shanping, LI Dianzhong, LI Yiyi (Shenyang National Laboratory for Materials Science, Institute of Metal Research, Chinese Academy of Sciences, Shenyang 110016, China). p 45 - 48

Abstract: Tungsten particles were chosen as the trace-element to investigate the pattern of the Marangoni convection on the pool surfaces of conventional TIG and double shielded TIG weld and to study the mechanism of the TIG weld shape variation. Before welding, the 300 - 500 micron size tungsten particles were uniformly smeared on the surface of work piece which were inserted two tungsten plates at the pool bottom to separate the weld pool center area and the edge region. For conventional TIG welding process, outward Marangoni flow existed on the pool surface and the tungsten particles concentrated in the two edges at the pool bottom. For double shielded TIG process, an inward Marangoni convection on the molten pool surface and tungsten particles located on the pool center between the two tungsten plates. Tracer test proved the flow direction of the weld pool in the TIG process and verified the active element could change the direction of the Marangnon convection.

Key words: TIG welding; tracer test; Marangoni convection; tungsten particles

Numerical analysis of residual stress on magnesium alloy and stainless steel butt joint by hybrid laser-TIG welding LI Xunbo[1], WU Gang[1], ZENG Zhi[1], WANG Jinxia[2], ZHAO Gang[2] (1. School of Mechatronics Engineering, University of Electronic Science and Technology of China, Chengdu 611731, China; 2. Chengdu Hanyan Weida Automatic Welding Equipment Co., Ltd, Chengdu 610300, China). p 49 - 52

Abstract: The AZ31B magnesium alloy and 304L stainless steel butt joint were obtained in laser-TIG hybrid welding. A new coupled heat source model was developed, which combined by double-elliptic planar distribution, double-ellipsoid body distribution and Rotary-Gauss body distribution model. The thermo-mechanical behavior and residual stresses distribution of the butt joint were analyzed by using finite element techniques. The results show that the temperature distribution of the dissimilar metal hybrid weld joint is different, and the residual stress on the 304L stainless steel plate is lower than that on the AZ31B magnesium plate.

Key words: magnesium alloy; stainless steel; hybrid welding; residual stress

Solderability and microstructure of Sn-9Zn-xPr lead-free solder XUE Peng[1], XUE Songbai[1], SHEN Yifu[1], YE Huan[1], XIAO Zhengxiang[2] (1. College of Materials Science and Technology, Nanjing University of Aeronautics and Astronautics, Nanjing 210016, China; 2. Sany Heavy Industry Co., Ltd, Changsha 410100, China). p 53 - 56

Abstract: The effects of Pr on the wettability of Sn-9Zn lead-free solder and the mechanical properties of soldered joints are investigated and the results indicate that with the addition of rare earth Pr into Sn-9Zn solder, the microstructure is refined obviously, Zn-rich phrase is decreased and mechanical properties